Available online at www.sciencedirect.com
ScienceDirect
Journal of Catalysis 251 (2007) 315–320
JOURNAL OF CATALYSIS
www.elsevier.com/locate/jcat

Synthesis and characterization of Al_2O_3 and ZrO_2–TiO_2 nano-composite as a support for NO_x storage–reduction catalyst

Haruo Imagawa *, Toshiyuki Tanaka, Naoki Takahashi, Shin'ichi Matsunaga, Akihiko Suda, Hirofumi Shinjoh

Toyota Central Research and Development Labs., Inc., 41-1 Yokomichi, Nagakute, Nagakute-cho, Aichi 480-1192, Japan

Received 11 June 2007; revised 7 August 2007; accepted 7 August 2007

Available online 12 September 2007

Abstract

To improve the thermal stability of NO_x storage–reduction catalysts, a novel support containing Al_2O_3, ZrO_2, and TiO_2 was synthesized by the coprecipitation method. The XRD and TEM results indicated that primary particles of γ-Al_2O_3 and a solid solution of ZrO_2–TiO_2 coexisted as secondary particles, that is, the synthesized support was a nano-composite of γ-Al_2O_3 and ZrO_2–TiO_2. The synthesized support had a characteristic single meso-pore, derived from the structure of the secondary particle. The basicity of the synthesized support was lower than that of the physically mixed oxide. After thermal treatment, aggregation of the ZrO_2–TiO_2 particles in the support was inhibited relative to that in the mixture of Al_2O_3 powder and ZrO_2–TiO_2 powder. This was attributed to the diffusion barrier (against ZrO_2–TiO_2) created by primary Al_2O_3 in the synthesized support. After a thermal aging test, the NO_x storage–reduction catalyst containing the synthesized support had a larger NO_x storage capacity than the catalyst containing the physically mixed oxide.

Keywords: Nano-composite; Alumina; Zirconia; Titania; Solid solution; Thermal stability; NO_x storage–reduction catalyst; Lean-burn engine

1. Introduction

In an effort to protect the environment, and minimize the effects of greenhouse gases, a reduction in the emission of carbon dioxide (CO_2) from automobiles is necessary. The lean-burn engine system is one of the most effective methods to improve the fuel efficiency of vehicles. However, one major drawback of this system is that conventional three-way catalysts cannot reduce nitrogen oxides (NO_x) into nitrogen (N_2) due to the existence of excessive oxygen in the exhaust gases. A number of catalyst systems have been explored to reduce NO_x in lean systems [1–3].

The NO_x storage–reduction catalyst (NSR catalyst) is one of the most attractive methods to purify exhaust gases from the lean-burn engine [4,5]. The mechanism of the NO_x storage and reduction reactions on the NSR catalysts is as follows [6]. First, during the lean condition, excess NO_x is oxidized to NO_2 on the precious metals and stored in the form of nitrate in storage materials. Second, when the engine is switched to operate on a rich air-fuel ratio, nitrate stored in the storage material is reduced to N_2 by hydrogen (H_2), carbon monoxide (CO), and hydrocarbons (HC).

The NSR catalyst has two main technical problems: sulfur poisoning and thermal deterioration. Sulfur dioxide (SO_2) contained in gas exhaust reacts with the storage materials and forms sulfate. However, recent studies on sulfur durability have reported that TiO_2 in supports has been found to be provide a high tolerance against sulfur poisoning due to its high acidity [7].

Thermal deterioration of the catalyst occurs due to both solid-phase reaction of NO_x storage materials with TiO_2 and aggregation of the support particles. In an effort to avoid solid-phase reaction, ZrO_2 is typically added as ZrO_2–TiO_2 solid solution [6,8]. On the other hand, Al_2O_3, which has excellent thermal stability, is added to the support. Typically, Al_2O_3 is physically mixed with other support materials, and does not contribute to the thermal stability of other support components. Nano-composites of Al_2O_3 and CeO_2–ZrO_2 solid solution have

* Corresponding author. Fax: +81 561 63 6136.
E-mail address: e1152@mosk.tytlabs.co.jp (H. Imagawa).

0021-9517/$ – see front matter
doi:10.1016/j.jcat.2007.08.002

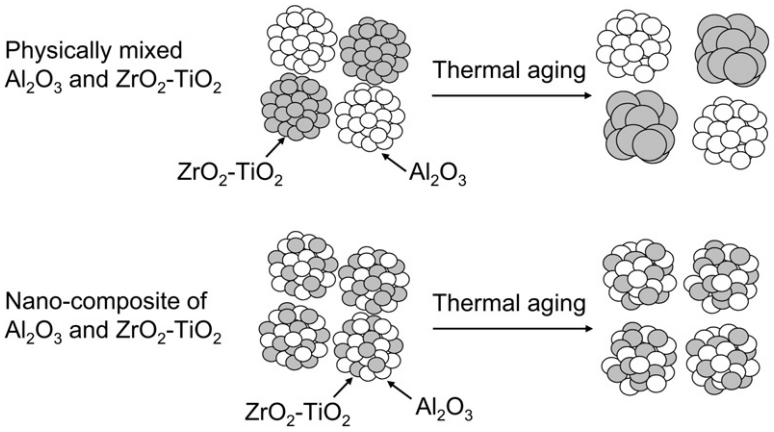

Fig. 1. Concept chart of the nano-composite of Al_2O_3 and ZrO_2–TiO_2.

been used as a support for three-way catalysts, and have been shown to inhibit the thermal aggregation of CeO_2–ZrO_2 [8], because Al_2O_3 acts as the diffusion barrier for CeO_2–ZrO_2 particles in the secondary particles. As a result, particle growth of not only CeO_2–ZrO_2, but also precious metals on the supports is prevented. This concept of the nano-composite can be applied to ZrO_2–TiO_2, that is, the thermal aggregation of ZrO_2–TiO_2 particles may be inhibited in the presence of Al_2O_3 particles (Fig. 1).

The purpose of this investigation is to improve the thermal stability of a support for NSR catalysts. In this work, the effects of the novel support on the thermal stability in both powder and catalyst are examined.

2. Experimental

2.1. Preparation of supports

The nano-composite oxide containing Al_2O_3, ZrO_2, and TiO_2 was prepared by conventional coprecipitation. $Al(NO_3)_3 \cdot 9H_2O$, $ZrO(NO_3)_2 \cdot 2H_2O$, and $TiCl_4$ (Wako Pure Chemical Industries) were dissolved in ion-exchanged water, and then an ammonia solution was added for coprecipitation. The obtained product was dried at 673 K for 5 h and calcined at 1073 K for 5 h in air. The weight ratio of Al_2O_3 to ZrO_2–TiO_2 was 50:50. The mole ratio of ZrO_2 to TiO_2 was 60:40, which showed maximal durability against heat [6].

Pure γ-Al_2O_3 was prepared by the same method. Pure ZrO_2–TiO_2 was prepared by the same method, as reported in literature [6]. Reference support was obtained by physically mixing pure γ-Al_2O_3 and ZrO_2–TiO_2. The composition of the physically mixed oxide was the same as that of the nano-composite oxide.

2.2. Characterization of supports

The crystal structure was characterized by powder X-ray diffraction (XRD). XRD patterns were recorded using a Rigaku RINT-2100 (Cu$K\alpha$ radiation ($\lambda = 1.5418$ Å), 40 kV, 30 mA). To analyze the distribution of Al_2O_3 and ZrO_2–TiO_2, field-emission transmission electron microscopy (FE-TEM) was performed on a Hitachi HF-2000.

The BET surface area was measured by N_2 adsorption at 77 K using Micro Data MICRO SORP 4232II.

The pore size distribution was calculated from the intrusion curve obtained with a mercury porosimetry using Quantachrome Pore Master GT60-1.

The surface acid–base properties of the supports were measured by NH_3- and CO_2-temperature programmed desorption (TPD). Samples were formed into 0.3–0.7 mm diameter pellets. In NH_3-TPD, after pretreatment at 773 K under a N_2 atmosphere, NH_3 was added in the stream of N_2 at 373 K, and then samples were heated to 773 K at a rate of 20 K/min. NH_3 desorbed from samples under the N_2 atmosphere was observed using a non-dispersive infrared (NDIR) type analyzer, Best Sokki CATA5000. CO_2-TPD was measured in the same method with NH_3-TPD. Helium (He) was used as balance gas instead of N_2, and desorbed CO_2 was observed using a NDIR type analyzer, Horiba MEXA-7100.

2.3. Analysis of supports after thermal treatment

Samples used were heated at 1073, 1173, and 1273 K for 5 h in air containing 3% water. The crystal structure after thermal treatment was analyzed by XRD and the particle size of ZrO_2–TiO_2 was calculated using Scherrer's formula [9]. The samples calcined at 1173 K were analyzed by FE-TEM in order to investigate the state of ZrO_2–TiO_2.

2.4. Catalytic application

Catalysts were prepared by impregnating $Pt(NH_3)_2(NO_2)_2$ and $Rh(NO_3)_3$ (Tanaka Precious Metals), then dried at 383 K for 12 h and finally calcined at 523 K for 3 h in air. The loading amounts of platinum and rhodium were 1.23 and 0.06 wt%. The powder obtained was then added to an aqueous solution containing $(CH_3COO)_2Ba$ and CH_3COOK (Wako Pure Chemical Industries) as precursors to the storage materials. The loading amounts of barium as BaO and potassium as K_2O were 18.8 and 5.8 wt%. After the catalysts were dried at 383 K for 12 h,

they were calcined at 773 K for 3 h in air. The powder obtained was formed into 0.3–0.7 mm diameter pellets.

In thermal aging tests, the catalyst was exposed to a feedstream as shown in Table 1, which simulated the actual engine exhaust gas, and heated at 1073 K for 5 h. The lean and rich atmospheres were switched every 2 min. The gas flow rate was 1000 cm^3/min and the gas hourly space velocity was 30,000 h^{-1}.

The amount of NO_x stored was measured using a conventional fixed-bed flow reactor system at atmospheric pressure. Table 1 shows the composition of the feedstreams simulating the actual engine exhaust gas for this measurement. After the catalyst was heated at 573 K under a rich atmosphere, the gas was switched to the lean atmosphere until the outlet NO_x concentration reached a constant value. Then a 3s-rich spike was introduced to the catalyst. Subsequently, the gas was switched to the lean atmosphere until the outlet NO_x concentration reached a constant value. The amount of NO_x stored was calculated as the difference in the NO_x amount between the inlet and the outlet gases after the rich spike. Measurement of the amount of NO_x stored at 673 and 773 K was similar to that at 573 K. The gas flow rate was 3000 cm^3/min and the gas hourly space velocity was 180,000 h^{-1}. The NO_x concentration was measured using a chemiluminescent NO_x meter attached to a Horiba MEXA-7100.

Table 1
Gas composition for thermal aging test and NO_x storage measurement

Atmosphere	C_3H_6 (%C)	CO (%)	H_2 (%)	NO (ppm)	CO_2 (%)	O_2 (%)	H_2O (%)
Thermal aging test[a]							
Lean	0.065	0	0	800	11	6.6	3
Rich	0.34	5.6	1.9	50	11	0	3
NO_x storage measurement[b]							
Lean	0.02	0	0	800	11	6.6	3
Rich	0.11	5.6	1.9	0	11	0.3	3
Rich spike	0.11	5.6	1.9	50	11	0	3

[a] N_2 balance.
[b] He balance.

The noble metal dispersion was obtained from CO pulse chemisorption at 323 K with Ohkura Riken R6015-S. The pulse gas was 100 vol% CO for fresh catalysts or 2 vol% CO in He for aged catalysts. The metal dispersion was calculated by assuming a CO to surface metal atom ratio of 1:1 [10].

3. Results and discussion

3.1. Analysis of the structure of the synthesized support

The XRD pattern of the sample is shown in Fig. 2. The synthesized support consists of an amorphous γ-Al_2O_3 phase and a crystalline tetragonal ZrO_2 phase after calcination at 1073 K. The peak assigned to tetragonal ZrO_2 (101) phase shifted from $2\theta = 30.22°$ to 30.42°. Therefore, this peak shift suggests that TiO_2 has been solved in the ZrO_2 phase and ZrO_2–TiO_2 solid solution has formed in the synthesis step.

The TEM image of the synthesized support is shown in Fig. 3. Al_2O_3 primary particle (pale gray particle) and ZrO_2–TiO_2 primary particle (dark gray and clear-shape particle) coexisted in the same secondary particles. Each of the primary particles was less than 20 nm. This structure is attributed to the condition under which precipitation of Al_2O_3 and ZrO_2–TiO_2 begins to develop at the same time. In brief, this novel synthesized support consists of a nano-composite of amorphous γ-Al_2O_3 and ZrO_2–TiO_2 solid solution (nano-composite oxide).

3.2. Characterization of the nano-composite oxide

3.2.1. Surface area

Fig. 4 shows the BET surface area at each calcination temperature. Even at 1073 K, the nano-composite oxide had a large surface area, approximately 130 m^2/g. Compared with the change of the BET surface area in pure ZrO_2–TiO_2, the surface area of the nano-composite oxide decreased linearly as the calcination temperature increased, and did not show a sharp drop between 873 and 973 K. This sharp drop in pure ZrO_2–TiO_2 results from the rapid crystallization and sintering of ZrO_2–TiO_2.

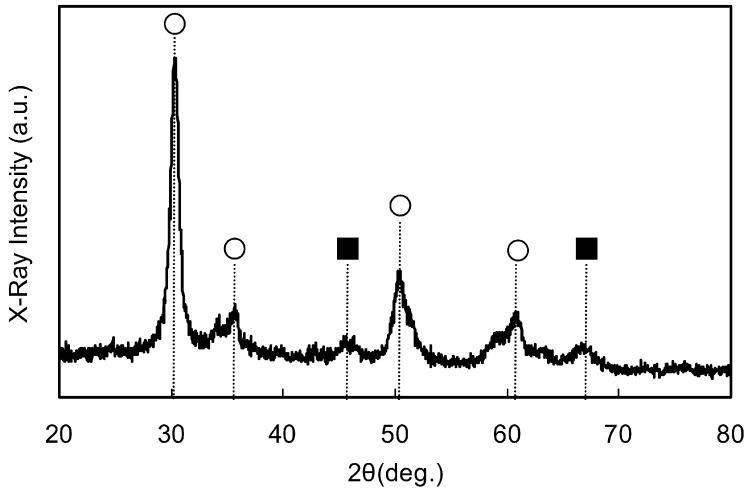

Fig. 2. XRD spectra of the nano-composite of Al_2O_3 and ZrO_2–TiO_2 calcined at 1073 K. (○) Tetragonal ZrO_2; (■) γ-Al_2O_3.

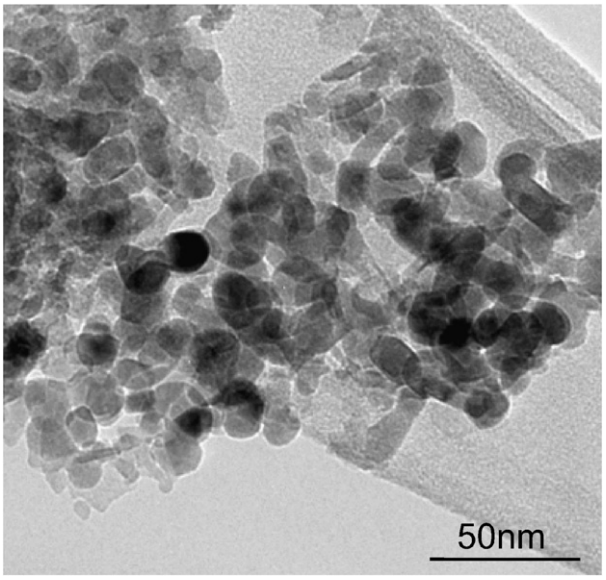

Fig. 3. FE-TEM micrograph of the nano-composite of Al_2O_3 and ZrO_2–TiO_2 calcined at 1073 K.

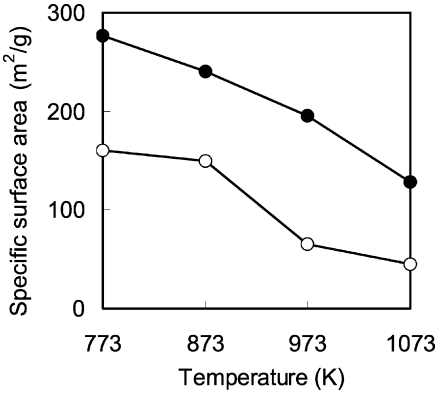

Fig. 4. BET-specific surface area of samples versus calcination temperature. (●) Nano-composite of Al_2O_3 and ZrO_2–TiO_2; (○) pure ZrO_2–TiO_2.

In the nano-composite oxide, the Al_2O_3 particle acts as the diffusion barrier of the ZrO_2–TiO_2 particle in the nano-composite oxide, which prevents rapid sintering of the ZrO_2–TiO_2 particle. Therefore, such a sharp drop of the surface area is prevented and a large surface area in the nano-composite oxide is maintained.

3.2.2. Pore diameter distribution

Fig. 5 shows the pore diameter distribution of each sample. The nano-composite oxide had a single sharp meso-pore around 15 nm (Fig. 5, black line). In the nano-composite oxide, Al_2O_3 and ZrO_2–TiO_2 exist in the same secondary particle and there is only one kind of pore in the secondary particle. This pore diameter distribution is in good agreement with that of the structure.

On the other hand, the mixture of Al_2O_3 and ZrO_2–TiO_2 (physically mixed oxide) had a broad pore distribution from 9 to 40 nm (Fig. 5, gray line). This broad distribution is brought about by the mixture of the two different kinds of pores derived from the Al_2O_3 secondary particle and ZrO_2–TiO_2 secondary particle. After calcination of the physically mixed oxide at 1073 K, two characteristic peaks were clearly observed (Fig. 5, black broken line). As the ZrO_2–TiO_2 particle is easily sintered with the increase in calcination temperature, the larger diameter peak is derived from the ZrO_2–TiO_2 secondary particle and the smaller one is derived from Al_2O_3 secondary particle.

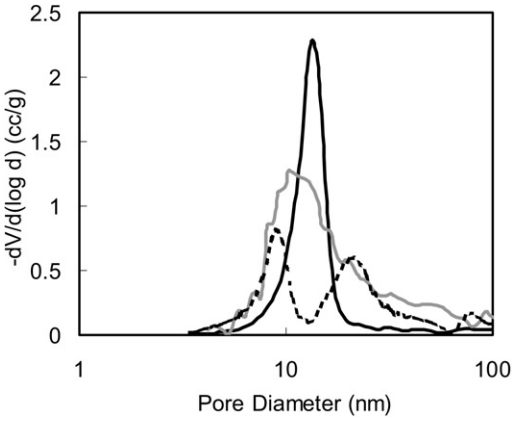

Fig. 5. Pore distribution of samples: nano-composite of Al_2O_3 and ZrO_2–TiO_2 calcined at 1073 K (—); physically mixed Al_2O_3 calcined at 1073 K and ZrO_2–TiO_2 calcined at 773 K (—); physically mixed Al_2O_3 and ZrO_2–TiO_2 calcined at 1073 K (- - -).

Table 2
Meso-pore volume and acid–base amount of samples

	Meso-pore volume (cc/g)	Acid amount (μmol/g)	Base amount (μmol/g)
Nano-composite oxide	0.415	96.7	2.7
Physically mixed oxide	0.318	105.4	12.1

The meso-pore volume after calcination at 1073 K is shown in Table 2. The nano-composite oxide had a larger meso-pore volume than the physically mixed oxide, because ZrO_2–TiO_2 particles in the nano-composite oxide has been inhibited from aggregating and held the large spacing among the primary particles.

3.2.3. Acid–base property

It has been reported that TiO_2 in supports has high tolerance against sulfur poisoning, because TiO_2 is one of the acidic oxides [7]. Therefore, in this system, TiO_2 is involved as a ZrO_2–TiO_2 solid solution. In an effort to observe the effect of the structure of the nano-composite oxide on the acid–base properties, the surface acidity and basicity were measured by a NH_3- and CO_2-TPD experiment, respectively.

Table 2 shows the amount of acid in each sample. The amount of acid in the nano-composite oxide was almost the same as those composed of the physically mixed oxide and both NH_3-TPD spectra had a peak around 450 K, indicating that the conformation of the Al_2O_3 particle and ZrO_2–TiO_2 particles had no effect on the acidity of the material.

In the CO_2-TPD spectra, the maximum CO_2 concentration of the nano-composite was quite smaller than that of the physically mixed oxide. Table 2 shows the amount of base determined by the CO_2 desorption from the samples. The amount of

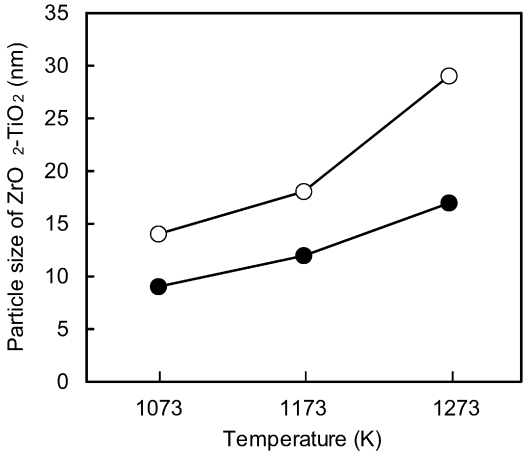

Fig. 6. Average particle size of ZrO_2–TiO_2 determined by XRD data versus thermal treatment temperature. (●) Nano-composite of Al_2O_3 and ZrO_2–TiO_2; (○) physically mixed Al_2O_3 and ZrO_2–TiO_2.

base in the nano-composite oxide was 1/5 times as large as that in the physically mixed oxide. This result suggests the possibility of inhibition of adsorption of SO_x on the surface in NSR catalysts using nano-composite oxide as a support.

The CO_2 adsorbed onto ZrO_2–TiO_2 is nearly negligible [6]. Therefore, the difference in the basicity between the nano-composite oxide and the physically mixed oxide is derived from the Al_2O_3 state. In the physically mixed oxide, CO_2 is easily adsorbed to the basic surface of the Al_2O_3 particle due to the pure Al_2O_3 secondary particle. On the other hand, in the nano-composite oxide, it can be inferred that the basicity of Al_2O_3 was decreased due to the existence of trace amounts of impurity such as TiO_2 and/or ZrO_2. The method of synthesizing the nano-composite oxide is coprecipitation, therefore, it is possible that a trace amount of Ti and/or Zr exist on the surface of the Al_2O_3 particle. However, the acidity of ZrO_2 is significantly lower than TiO_2, and ZrO_2 is highly basic [6]. On the other hand, TiO_2 has a high acidity and negligible basicity. Thus, the basicity of Al_2O_3 is canceled by the acidity of TiO_2 to some degree. To clarify this point, further experiments must be performed.

3.2.4. ZrO_2–TiO_2 particle after thermal treatment

Fig. 6 shows the average particle size for ZrO_2–TiO_2 determined by XRD after thermal treatment. At temperatures less than 1073 K, the particle size of the nano-composite oxide could not be determined with XRD because the ZrO_2–TiO_2 phase was amorphous. Therefore, the average particle size of ZrO_2–TiO_2 was examined at temperatures greater than 1073 K.

The particle size of ZrO_2–TiO_2 in the nano-composite oxide was smaller than that in the physically mixed oxide at each temperature measured. The difference in ZrO_2–TiO_2 particle size between the nano-composite oxide and the physically mixed oxide increased with the increase in temperature in the thermal treatment. At 1273 K, the ZrO_2–TiO_2 particle size in the nano-composite oxide was about half the size of that in the physically mixed oxide.

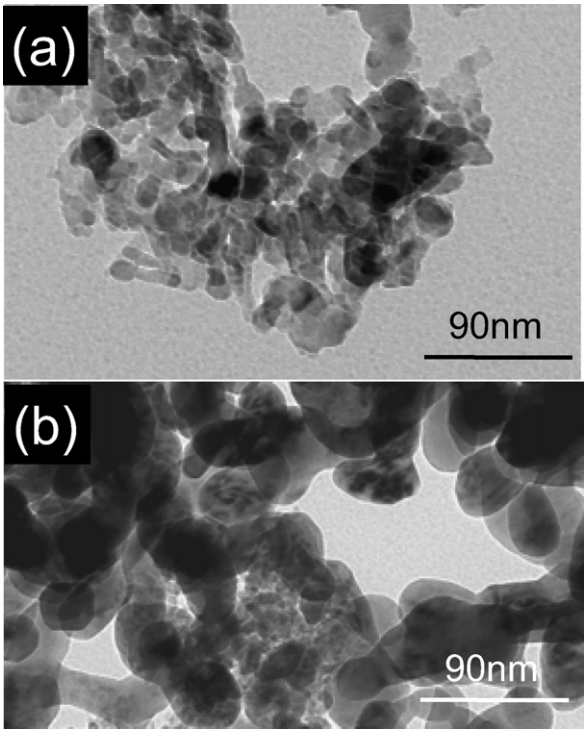

Fig. 7. FE-TEM micrographs of samples after thermal treatment at 1173 K. (a) Nano-composite of Al_2O_3 and ZrO_2–TiO_2; (b) physically mixed Al_2O_3 and ZrO_2–TiO_2.

Fig. 7 shows the TEM image after thermal treatment at 1173 K. In the nano-composite oxide (Fig. 7a), the particle size of the primary ZrO_2–TiO_2 particles was less than 30 nm on average. On the other hand, the aggregation of the ZrO_2–TiO_2 particles in the physically mixed oxide was observed compared with that in the nano-composite oxide (Fig. 7b).

ZrO_2–TiO_2 primary particles in the nano-composite oxide are surrounded by Al_2O_3 primary particles, which serve as the diffusion barrier for ZrO_2–TiO_2. Therefore, the aggregation of ZrO_2–TiO_2 primary particles by heat is inhibited in the nano-composite oxide in accordance with the concept showed in Fig. 1.

3.3. Catalytic application

To confirm the effect of thermal resistance of the nano-composite oxide as a support for a NO_x storage–reduction catalyst, the NO_x storage amount of catalysts thermally aged was measured. The NO_x storage amount at each temperature is shown in Fig. 8a and the NO_x concentration profile in the outlet gas at 673 K is depicted in Fig. 8b. The catalyst containing the nano-composite oxide (Cat. A) had larger amount of NO_x storage than that containing the physically mixed oxide (Cat. B). At 673 K, the NO_x storage of Cat. A was twice as large as that of Cat. B. The Ba and K species under lean condition are assumed to be nitrate species such as $Ba(NO_3)_2$ and KNO_3, as reported in literatures [5,11,12].

The particle size of ZrO_2–TiO_2 in catalysts was analyzed by XRD after a thermal aging test. Compared with the result at 1073 K in Fig. 6, the ZrO_2–TiO_2 particle size in the nano-

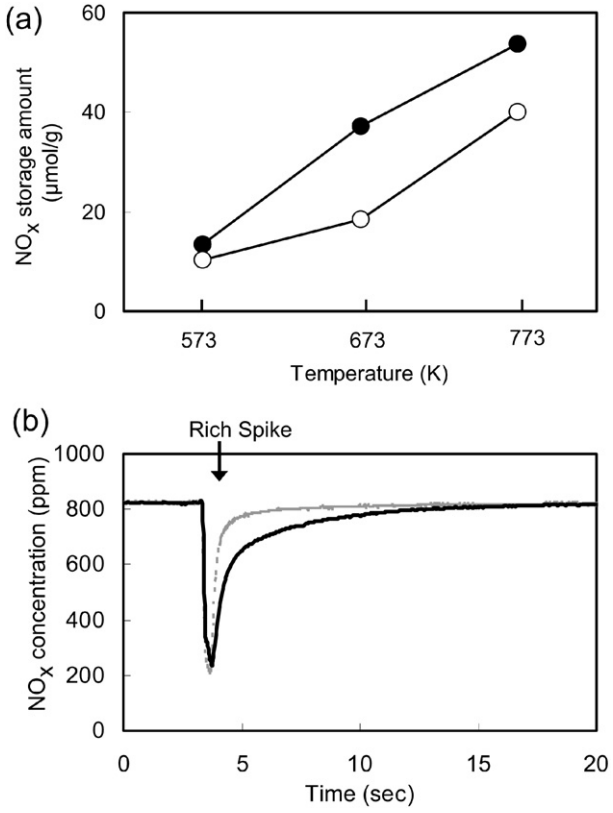

Fig. 8. (a) NO_x storage performance versus reaction temperature after thermal aging test: (●) Cat. A, catalyst using nano-composite of Al_2O_3 and ZrO_2–TiO_2 as a support; (○) Cat. B, catalyst using physically mixed Al_2O_3 and ZrO_2–TiO_2 as support. (b) NO_x concentration profile in the outlet gas at 673 K under lean-rich cycle after thermal aging test: Cat. A (—), Cat. B (- - -).

composite oxide was almost the same, even in the catalyst that underwent the thermal aging test. On the other hand, in the physically mixed oxide, the particle size of ZrO_2–TiO_2 became twice the size of the powder after the thermal aging test.

The aggregation and deterioration of precious metal on the nano-composite oxide are expected to be inhibited relative to those in physically mixed oxides. To confirm this point, the noble metal dispersion of catalysts was measured by CO pulse chemisorption. In fresh catalyst, the noble metal dispersion of Cat. A was 6.8% and that of Cat. B was 10.3%. But after thermal aging test, the dispersion of Cat. A was 2.5% and that of Cat. B was 1.3%. Therefore, Cat. A has a high density of catalytically active sites after thermal aging test relative to Cat. B.

For practical purposes, a NO_x storage–reduction catalyst is mainly exposed to temperatures such as 673 K [11], that is, nano-composite oxide is a promising material for high performance in real exhausted gases from lean-burn engines.

4. Conclusion

A nano-composite of γ-Al_2O_3 and ZrO_2–TiO_2 solid solution was synthesized. After thermal treatment, the aggregation of ZrO_2–TiO_2 particles in the nano-composite of Al_2O_3 and ZrO_2–TiO_2 was inhibited relative to that in the physically mixed Al_2O_3 and ZrO_2–TiO_2. This was thought to be because Al_2O_3 particles act as a diffusion barrier to ZrO_2–TiO_2 particles in the nano-composite oxide.

After a thermal aging test using simulated model exhausted gas from lean-burn engines, the catalyst containing the nano-composite oxide as a support for NO_x storage–reduction catalysts had a larger amount of NO_x storage than that containing the physically mixed oxide. This result suggests that using the nano-composite of Al_2O_3 and ZrO_2–TiO_2 as a support is a better method for a NO_x storage–reduction catalyst.

References

[1] S. Sato, Y. Yu, H. Yahiro, N. Mizuno, M. Iwamoto, Appl. Catal. 70 (1991) L1.
[2] Y. Kintaichi, H. Hamada, M. Tabata, M. Sasaki, T. Ito, Catal. Lett. 6 (1990) 239.
[3] R. Burch, P.J. Millington, Catal. Today 26 (1995) 185.
[4] W. Bögner, M. Krämer, B. Krutzsch, S. Pischinger, D. Voigtländer, G. Wenninger, F. Wirbeleit, M.S. Brogan, R.J. Brisley, D.E. Webster, Appl. Catal. B Environ. 7 (1995) 153.
[5] N. Takahashi, H. Shinjoh, T. Iijima, T. Suzuki, K. Yamazaki, K. Yokota, H. Suzuki, N. Miyoshi, S. Matsumoto, T. Tanizawa, T. Tanaka, S. Tateishi, K. Kasahara, Catal. Today 27 (1996) 63.
[6] N. Takahashi, A. Suda, I. Hachisuka, M. Sugiura, H. Sobukawa, H. Shinjoh, Appl. Catal. B Environ. 72 (2006) 187.
[7] S. Matsumoto, Y. Ikeda, H. Suzuki, M. Ogai, N. Miyoshi, Appl. Catal. B Environ. 25 (2000) 115.
[8] T. Kanazawa, Catal. Today 96 (2004) 171.
[9] Y. Xie, C. Yuan, Appl. Catal. B Environ. 46 (2003) 251.
[10] J.A. Anderson, R.A. Daley, S.Y. Christou, A.M. Efstathiou, Appl. Catal. B Environ. 64 (2006) 189.
[11] M. Takeuchi, S. Matsumoto, Top. Catal. 28 (2004) 151.
[12] N. Takahashi, K. Yamazaki, H. Sobukawa, H. Shinjoh, J. Chem. Eng. Jpn. 39 (2006) 437.